J Electroceram (2009) 22:47–54
DOI 10.1007/s10832-007-9381-2

Nanoblast synthesis and SPS of nanostructured oxides for SOFC

H. Borodianska · O. Vasylkiv · Y. Sakka

Received: 5 March 2007 / Accepted: 29 November 2007 / Published online: 18 December 2007

Abstract Engineering of Cerium Gadolinium Oxide (CGO) and Yttria Stabilized Zirconia (8Y-SZ) ceramic nanopowder with precise morphology and homogeneity of the compounds by multiple nanoblast technique of preliminary engineered nanoreactors was analysed. Nanoreactors were produced by morphology optimization technique and loaded by colloidal impregnation of the $C_3H_6N_6O_6$. The subsequent explosive initiation of $C_3H_6N_6O_6$ followed thermal detonation form gaseous products with local temperatures of ~2500°C. The rapid evolution of a large volume of gaseous products i.e. impacts of the blast waves dissipates the heat of the process and limits temperature increase, thus reducing the possibility of premature local partial sintering among the primary particles; and leads to the fragmentation of the surrounding agglomerates. Uniformly aggregated nanosize CGO and 8Y-SZ consisting of ~50 nm nano-aggregates of ~7 nm crystallites with a remarkably homogeneous composition and uniform morphology were synthesized. The SPS consolidation of nanosized aggregates of 8Y-SZ and CGO was analyzed. The 8Y-SZ ceramic with an average grain size of 90 nm and CGO nanoceramic with average grain sizes of 73, 32 and 12 nm were obtained by SPS at 1100, 1035 and 970°C, respectively under the pressures of 90–150 MPa.

Keywords Nanoblast synthesis · Nanoreactor · SPS · Nanopowder · Nanostructured ceramic · SOFC · Conductivity

H. Borodianska · O. Vasylkiv (✉) · Y. Sakka
National Institute for Materials Science,
1-2-1, Sengen,
Tsukuba, Ibaraki 305-0047, Japan
e-mail: oleg.vasylkiv@nims.go.jp

1 Introduction

Fabrication of nanopowders with uniform morphology and precise stoichiometry is a key to realizing high-performance devices based on nanostructured metal oxide ceramics for a wide range of applications [1–3]. Oxide ion-conducting solid electrolytes have found wide applications in energy conversion, combustion control, chemical processing, and electrochemical cells for measuring the oxygen activities and thermodynamic data of solid, liquid and gaseous phases. The highest possible ionic conductivity of the solid electrolyte is required for device performance. Y_2O_3-stabilized-ZrO_2 (Y-SZ) is the most common electrolyte among the entire ZrO_2-based electrolytes used in solid oxide fuel cells (SOFC) and oxygen sensors because of its adequate ionic conductivity, stability in a dual environment (oxidizing and reducing) and durability against reaction by-products at the electrodes. Its ionic conductivity is consistently higher than 0.1 S/cm at 1000°C, and the electronic conductivity is less than 10^{-4} S/cm over the entire oxygen potential region for the fuel cell operation [5]. CeO_2-based materials have been intensively investigated as oxide-ion conducting solid electrolytes in electrochemical cells. At the temperatures of 700–800°C, the rare-earth (RE)-doped ceria demonstrates higher oxide-ion conductivity than that of the yttria-stabilized zirconia [10–12].

Ceramic nanopowders are usually synthesized by several aqueous-solution-based precipitation techniques [1–19] which have included approaches based on sol–gel processing [5–26], a reverse-micellar nanoreactor [3, 4], hydrothermal synthesis [13–15], sonochemically and/or microwave-assisted decomposition of various aqueous (or non-aqueous) precursor solutions [15], salt-assisted aerosol decomposition and combustion synthesis [16–17]. However, due to the differences in the synthesis kinetic, high

surface energy of the nanoparticles, and its chemical activity, hard agglomeration and the compositional inhomogeneity are the main problems encountered in nanosynthesis [1, 6–15, 18–26].

One possibility of solving these problems is an elaboration of the nanoparticles synthesis process inside the confined multifunctional microreactors i.e. a polyelectrolyte capsules with controlled shell permeability and the possibility of shell engineering on the nanolevel, thus tailoring different functionalities [21]. The main disadvantage of such a methodology is an extremely low productivity of these kinds of microreactors.

The first aim of the present study was an establishing of a synthetic technique which will allow the development of thermo-activated synthesis processes of the final compositions within the preliminary localized volume of single nanoreactors. Based on our opinion, this should provide the heredity of the final structure and chemical homogenity of the nanosize products.

For the thermal decomposition of preliminary engineered nanoreactors in this study, we employed the recently developed nanoblast technique [18, 19]. Explosions involve a rapid and violent oxidation reaction with a sudden release of mechanical and chemical energy in a violent manner, accompanied with the generation of a high temperature and the release of extremely hot gases. It causes pressure waves in the local medium in which it occurs.[21] Cyclotrimethylene trinitramine, used in this study, is an explosive material in its pure synthesized state, is a heterocycle and thus ring-shaped with the following structural formula: hexahydro-1,3,5-trinitro-1,3,5-triazine or $(CH_2\text{-}N\text{-}NO_2)_3$ [20]. At room temperature, it is extremely stable, non-soluble in water but partially soluble in ethanol. Its thermal decomposition starts at about 170°C, melting at 204°C, and it become explosive at 233°C [18, 19].

The second aim of the present study was to produce nanograined ceramics from preliminary engineered morphologically and compositionally homogeneous nanosize 8Y-SZ and CGO powders using a low-temperature spark plasma sintering (SPS) technique. This approach involves the rapid heating of a powder by an electric current with the simultaneous application of an external pressure. Numerous experimental investigations point to the ability of SPS to render highly-dense powder products with the potential of grain size retention. The latter ability is of significance for the consolidation of nano-powder materials, where the grain growth is one of the major problems [22–27].

2 Experimental procedure

$ZrO(NO_3)_2{\cdot}nH_2O$ (99.9% pure and produced by Wako Pure Chemicals Co., Japan), and YCl_3 produced as described elsewhere[14] were weighed and dissolved in water at a total concentration of 0.2 M. The initial amount of zirconium and yttrium compounds varied according to the concentrations of both compounds in the resulting alloys. The preparation conditions of the 8Y-SZ nanopowder were well described in earlier papers [14, 15]. Urea (NH_2CONH_2 99% pure and produced by Wako Pure Chemicals Co., Japan) was used as a precipitation agent in the present study.

For the $Gd_{20}Ce_{80}O_{1.90}$ (CGO) synthesis, $CeCl_3{\cdot}7H_2O$, and $GdCl_3{\cdot}6H_2O$ (both 99.9% pure from Wako Pure Chemicals Co., Osaka, Japan) were weighed and separately dissolved in doubly distilled and deionized water at a concentration of 0.2 M. The initial amount of the cerium and gadolinium compounds varied according to the concentrations of both ceramic oxides in the resulting solid solution.

To produce intermediate nanoreactors, i.e., complex bimetal aggregates, NH_2CONH_2 was dissolved in deionized water at the concentration of 2 M per $1–x$ M of $ZrO(NO_3)_2{\cdot}nH_2O$ or $CeCl_3{\cdot}7H_2O$ and xM $GdCl_3{\cdot}6H_2O$. Two jars with the total volume of the NH_2CONH_2 aqueous solution of 300 ml (200 ml for zirconium oxynitrate solution with 50 ml of yttrium chloride solution added for the 8Y-SZ preparation or cerium chloride, and 100 ml for the gadolinium chloride solutions) were prepared.

Both types of nanoreactors were synthesized as follows:

1. To produce the matrix porous aggregates, nucleation of the zirconium and cerium oxide in the aqueous solution was conducted by spraying 200 ml of a urea aqueous solution into the $ZrO(NO_3)_2{\cdot}nH_2O$ or cerium chloride aqueous solution. $CeCl_3{\cdot}7H_2O$ solution was heated to 80°C with stirring at 1,000 rpm and mixed under the prescribed conditions for 10 h. The gadolinium complex was nucleated by spraying the gadolinium chloride aqueous solution into a rapidly stirred (1,600 rpm) suspension of the as-synthesized cerium oxide. Because of the existence of residual non-reacted urea, decomposition began immediately upon starting the gadolinium chloride solution spraying. After 30 min, 100 ml of the urea solution was added by spraying into the stock suspension. Subsequent stirring at 80°C for five more hours was conducted to finalize the synthesis and homogenize the suspension. Finally, the product was washed with water followed by re-dispersion (according to [14]) of the soft agglomerates of the cerium and gadolinium intermediate compounds in ethanol (C_2H_5OH, 99.5% reagent grade, Kanto Chemicals, Japan) using an ultrasonic horn (Model USP-600, Shimadzu, Kyoto, Japan).

For the zirconia synthesis, stock aqueous solutions of concentration 0.1 M of Zr^{4+} +3 mol% of $2Y^{3+}$ were produced for the preparation of powder characterization

samples and maintained by magnetic stirring at 20°C (room temperature) for 24 h for the best homogenization. The 250 ml of mixed urea-containing sol in which the initial pH was ~1.2 after homogenization, was hydrothermally treated. Each sample was filled to 80 vol.% in a 250 ml Teflon vessel held in an outer pressure vessel made of stainless steel. After the vessel had been sealed, it was heated to 155°C for 50 h. Fifty hours is a total duration of the hydrothermal treatment. The urea decomposed into NH_3 and CO_2 through reaction with H_2O and the sol's pH changed to ~8.5. The homogeneous precipitate formed was hydrous yttria-doped ZrO_2, which crystallized under hydrothermal conditions.

2. To produce cyclotrimethylene trinitramine ($C_3H_6N_6O_6$), hexamethylenetetramine was dissolved in deionized water at the concentration of 0.1 M. Concentrated (~93%) nitric acid (from Wako Pure Chemicals Co., Osaka, Japan) was added to the urotropin solution. Mixing urotropin with nitric acid causes the formation and precipitation of cyclotrimethylene trinitramine ($C_3H_6N_6O_6$) [18–20]. Mixing the dissolved hexamethylenetetramine with diluted nitric acid causes the formation of well-dispersed nanoparticles of the $C_3H_6N_6O_6$ in the solvent.
3. Nanoreactors were produced by dissolving the cyclotrimethylene trinitramine in ethanol with subsequent loading of the porous uniform matrix aggregates of the complex cerium–gadolinium intermediate compounds with the finest particles of $C_3H_6N_6O_6$. Subsequently, loaded with explosive compound nanoreactors were slowly dried in a drying oven at 70°C and redispersed with no additional washing. The final multiple nanoblast synthesis was conducted in the similar manner as previously described [18, 19].

A spark plasma sintering system (Sumitomo Coal Mining SPS system, Dr. Sinter Model 1050, Japan) was used to prepare the SPS consolidated compacts. The powders were loaded into a graphite die (10 mm in diameter) and punch unit. In a typical densification experiment, 0.3–0.5 g of the ceramic nano-powders or pressed and subsequently CIPed in 400 MPa powder cylinders were loaded into the die which was then placed inside the SPS apparatus. All synthesized powders included in Table 1 were all characterized as having primary crystallite size below 10 nm.

A low pressure was initially applied. The vacuum level of the chamber was 4.5 Pa for the powder densification, and the applied compression was 25 MPa. The powder was first heated to 600°C (the lowest controllable temperature of SPS) at the heating rate of 200°C/min and then heated to the set temperature at various heating rates in the starting current range of 600–1,000 Å as listed in Table 2. The corresponding voltage lies between 3.0 and 4.5 V, respectively. The electric current was periodically pulsed at 14 pulses/s (2 of 14 pulses off as a recovery time). The temperature was measured using a pyrometer placed in hole on the surface of the graphite die cylinder. The heating rates were 400 and 500°C/min; the dwell time was 1 min.

After holding the powder samples (either just poured into the die or initially prepressed and CIPed) at the desired temperature in the range of 900–1250°C, and pressure range of 30–150 MPa, the applied electric current was stopped, the pressure was released, and the sample was gradually cooled to 600°C at the cooling rates of 10–100°C/min and subsequently furnace cooled to room temperature.

The relative density of the $Gd_{20}Ce_{80}O_{1.90}$ and fully stabilized cubic zirconia ceramics (8 mol% yttria 92 mol% zirconia) were based on 7.246 and 5.89 g/cm^3, respectively. The particle-size distribution was analyzed by the dynamic light scattering method (DLS) using a laser particle-size analyzer (Model LSPZ-100, Otsuka Electronics, Osaka, Japan). A very small amount of each powder (~5 mg) was dispersed in the distilled water for the analysis. Observation via TEM (Model JEM-2100-F, JEOL, Tokyo, Japan) operated at 200 kV was used to determine the nanoreactors and final powders morphologies. Phase identification of the powders and distribution of the components in each aggregate were determined by a nano-area energy dispersion X-ray spectroscopy analyzer (TEM-EDX). In addition to TEM, for analyzing the sintered ceramic, a Hitachi FESEM S-4800 operated at 5 kV and 200 nÅ was used. No conductive coating was applied on the fracture surface. The average grain size was determined from high-resolution SEM images of the fracture surfaces. The determination of the grain size in the densified nanometric oxides in a range below 50 nm is particularly challenging. Most of the traditional and well-established ceramographic techniques

Table 1 The size distribution of the bi-component intermediate cerium–gadolinium compounds and three-component nanoreactors loaded with the $C_3H_6N_6O_6$, as synthesized, after multiple nanoblast calcinations at 450°C with 30-min finalization holds.

Composition	Engineered nanoreactors (nm)	Aggregate size distribution after nanoblast treatment (nm)	Aggregate size distribution after calcination at 450°C (nm)	Primary crystallite size distribution (nm)
$Gd_{20}Ce_{80}O_{1.90}$ without $C_3H_6N_6O_6$	17–83	–	22–74	3–7
$Gd_{20}Ce_{80}O_{1.90}$ with $C_3H_6N_6O_6$	22–110	18–67	–	4–8

Table 2 Characteristics of the 8Y-SZ and the CGO powders, SPS details, and properties of consolidated ceramics.

Composition	Average aggregate size (nm)	Average primary crystallite size (nm)	Heating rate (°C/min)	CIP at 400 MPa	Hold temperature during SPS (°C)	Relative density (%)	Average grain size (nm)
8Y-SZ	~90	~9	400	No	1250	~96.3	~1,170
				Yes	1100	~89.2	~83
				Yes	1150	~98.9	~94
$Gd_{20}Ce_{80}O_{1.90}$ (no nanoblast treatment)	~70	~5	500	No	1100	~84.8	~161
				Yes	1100	~92.3	~176
				Yes	1035	~96.7	~123
$Gd_{20}Ce_{80}O_{1.90}$ nanoblast calcinations	~45	~6	500	No	1100	~89.1	~79
				Yes	1100	~93.8	~73
				Yes	1035	~97.9	~30
				Yes	970	~95.6	~12

cannot be used in this range. It is already known [27] that thermal etching of polished surfaces cannot be performed on these samples as the high temperatures required by this process can produce a significant alteration of the grain size. Moreover, it is also recognized that polishing can produce a significant stress-induced peak broadening in zirconia and other ceramics.[27] In samples with grain sizes below 50 nm, the stress cannot be annealed out without producing a modification in the grain size.

3 Results and discussion

3.1 Production of 8Y-SZ dense aggregates via preliminary engineered nanoreactors

To attain the highest possible compliance between the primary crystallite size and powder morphology the initial nanopowders of 8Y-SZ and CGO were produced via nanoreactor engineering technique.

After hydrothermal treatment at 155°C for 5 h, the aqueous sol of yttrium–zirconium intermediate complex was rapidly cooled and removed from the Teflon vessel. The ultrasonic dispersion for 1 min was applied to destroy the initial soft contacts between the as-nucleated and clustered yttrium–zirconium compounds. The produced extremely stable (no precipitation for 100 h was detected at pH 10) aqueous suspension was then poured into a Teflon vessel again and mounted on the magnetic stirrer. Suspension was then intensively stirred for next 45 h at 155°C. After cooling and subsequent washing, the produced uniformly aggregated 8 mol% yttria 92 mol% zirconia hydrous particles where analyzed by TEM and a nano-area energy dispersion X-ray spectroscopy analyzer (TEM EDX) which confirmed the morphological and compositional homogeneity of the as-synthesized yttrium–zirconium intermediate nanoreactors. The uniformity of morphology of the hydrous yttria-doped zirconia aggregates which consist of very fine primary particles, is shown on Fig. 1. The TEM-EDX mapping image of the hydrothermally synthesized 8Y-SZ intermediate nanoreactors (Fig. 2) shows the remarkably homogeneous distribution of yttrium within the zirconium matrix aggregates.

The following calcination at 600°C for 30 min resulted in uniformly shaped dense aggregates of fully stabilized cubic zirconia. A TEM micrograph of the 8 mol% yttria-stabilized zirconia (8Y-SZ) nano-powder is shown in Fig. 3. The primary crystallites with an average size of ~9 nm are aggregated into secondary nano-aggregates with a mean aggregate size of 30–110 nm. The satisfactory heredity of the final nano-aggregates morphology can be observed in Figs. 1 and 3. Such morphology is extremely important to prepare the uniform green samples which are only acceptable for subsequent low-temperature sintering.

3.2 Nanoblast synthesis of CGO nanopowders from preliminary engineered nanoreactors

The synthesis of the gadolinium oxide was conducted by direct spraying the gadolinium chloride aqueous solution into the as-synthesized cerium oxide suspension. The primary particles of

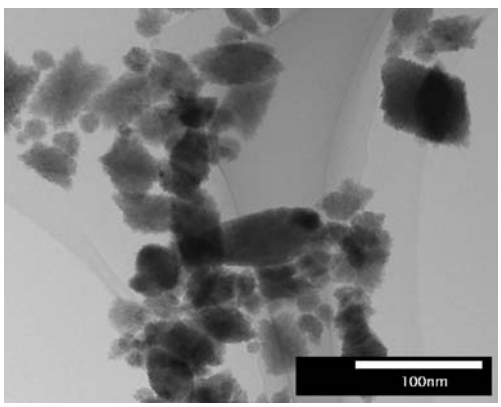

Fig. 1 Nanoreactors—engineered aggregates of yttria–zirconia intermediate compounds

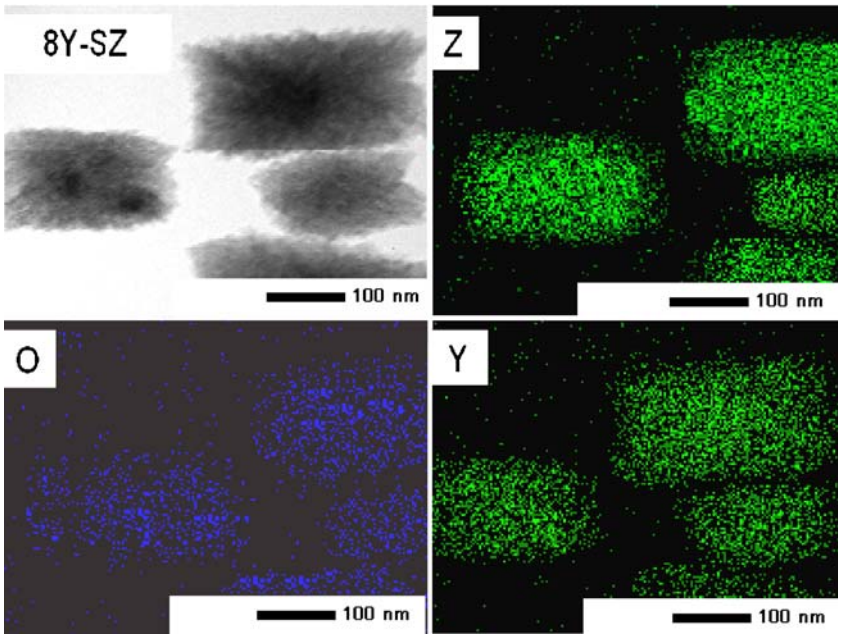

Fig. 2 TEM EDX maping of yttria–zirconia intermediate nanoreactors

the as-synthesized ceria assembled into fine aggregates covered with the as-synthesized clusters of the gadolinium intermediate complex that formed the matrix bi-metal nanoreactors. Table 1 shows the size distribution for bi-component intermediate cerium-gadolinium compounds and three-component nanoreactors loaded with $C_3H_6N_6O_6$, as synthesized, after multiple nanoblast calcinations at 450°C with 30-min finalization holds. This table includes particle size data for the as-synthesized nanoreactors, particle size distribution after the calcinations (in case of thermal decomposition of engineered bi-component nanoreactors) and, finally, characteristics of the powders produced by multiple nanoblast calcination/deagglomeration from nanoreactors loaded with cyclotrimethylene trinitramine. In both cases, the temperature of the calcination was 450°C with 30-min holds.

Prior to the calcinations both of the well-dried powders which composed of the bi-metal complex intermediate aggregates and the same aggregates, but additionally loaded with $C_3H_6N_6O_6$ that were briquetted by uniaxial pressing at

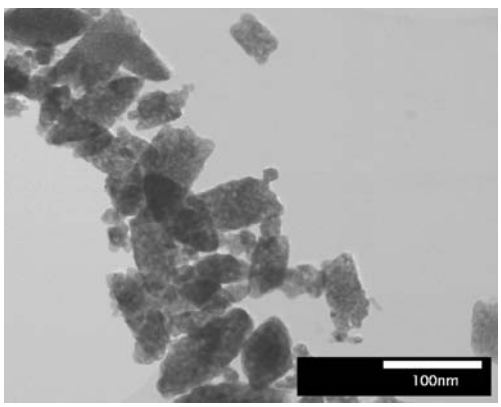

Fig. 3 The 8Y-SZ engineered nano-aggregates

4 MPa and separately filled into an alumina container for further thermal treatment. In the case of applying the nanoblast technique, prevention of the undesirable ignition of the $C_3H_6N_6O_6$ was extremely important [18–20]. For this reason ultra-rapid heating of the loaded nanoreactors through the thermal detonation temperature (~230°C for cyclotrimethylene trinitramine) was applied. This thermal detonation temperature, i.e., the temperature at which spontaneous multiple ruptures of the $N–NO_2$ bonds occur, strongly depends on the heating rate which may vary from 220 to 360°C. Extremely rapid detonation (10^{-8} s/g) of $C_3H_6N_6O_6$ separated into the porous matrix ceramic aggregates (i.e., nanoreactors) forms gaseous products with a temperature of 2500°C compressed into localized volumes equaling the initial volumes of each explosive particle. Multiple nanoblasts occur within the volume of the three-component nanoreactors. The instantaneous power of each blast is 500 MW/g [20]. The multiplied local impacts of the nanoblast waves lead to the fragmentation of the surrounding matter, i.e., deagglomeration of the powder. The rapid evolution of a large volume of extremely hot gaseous products dissipates the heat of the process and limits the temperature increase to localized areas. The last circumstance reduces the possibility of premature local partial sintering among the neighboring crystallites resulting in a non-agglomerated product. In addition, due to the short-term high temperature generation, which enhanced the solubility of the components, nanosize solid solution of the dopant gadolinium oxide into the matrix cerium oxide was synthesized. Utilizing the described technique, non-agglomerated cerium-gadolinium oxide (CGO) powder (Fig. 4) with an average primary crystallite size range of 3–9 nm, and an aggregate size of ~45 nm (see Table 2) was produced.

3.3 SPS consolidation of produced 8Y-SZ and CGO nanopowders

Finally, the consolidation of the powder samples of 8Y-SZ and CGO by spark plasma sintering (with and without preliminary CIPing) under different temperature/time conditions, pressures and starting current was analyzed with aim of obtaining highly dense nanograined ceramics. The applied pressures range was 30–150 MPa. The characteristics of the starting powders were thoroughly controlled.

The characteristics of the ceramics consolidated using the SPS technique are listed in Table 2. This table shows the average aggregate and crystallite sizes of the 8Y-SZ and CGO ceramic nanopowders obtained by the techniques described in Sections 3.1 and 3.2.

The SEM micrograph of the 8YSZ ceramic consolidated by SPS at 1250°C for 5 min is shown on Fig. 5. Such a relatively coarse-grained ceramic was obtained due to the use of the 8Y-SZ powder sample with no preliminary CIPing, those reducing the possibility of the SPS temperature lowering. It was studied earlier [8] that minor addition (~1 mass.%) of γ-Al_2O_3 particles in case of its uniform mixing with zirconia nanopowder enhance sinterability and significantly lower the sintering temperature. For attainment higher density with finer grain size, 1 mass.% of alumina powder was colloidally mixed in ethanol suspension with 8Y-SZ nanopowder prior to consolidation. In addition to doping with 1 mas.% of γ-Al_2O_3, pretreatment of the green samples by CIP at 400 MPa allowed significant reduction of the SPS consolidation temperatures. The SEM micrograph of the 8Y-SZ doped with 1 mas.% of alumina consolidated by SPS at 1150°C for 5 min is shown in Fig. 6. Comparing the average grain size of the 8Y-SZ ceramic after SPS consolidation with the initial average aggregate size, it is evident that the grain growth is very limited. Actually, we can conclude that only intra-aggregate recrystallization occurs and subsequently each aggregate became a single grain (See Table 2 and Fig. 6). However, due to shortening of high-temparature treatment during SPS consolidation the attained network of boundaries between the primary crystallites (or grains), i.e. the primary elements of each aggregate can be well defined from Fig. 6 as well.

During the sintering process, the pressure increases from 30 MPa while reaching 100 MPa at a maximum temperature with a subsequent gradual rise to 150 MPa during the 5-min holds. The pressure maximum of 150 MPa was applied at the punch unit for all samples either preCIPed or just poured powder samples. The electric current employed was typically 600–900 Å at 600°C which corresponds to 400–600 Å at the holding temperatures. The last condition means that the current gradually decreases with the increasing temperature and sample density. As shown in Table 2, the relative densities of the 8Y-SZ ceramic samples cold isostatically pressed and sintered at 1100 and 1150°C (both heated to the hold temperature at 400°C/min) were

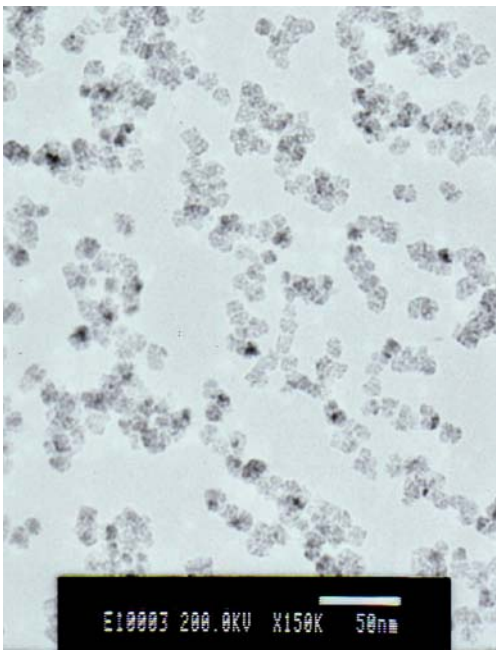

Fig. 4 The CGO non-agglomerated nanoparticles explosively calcined from the preliminary engineered nanoreactors impregnated with the $C_3H_6N_6O_6$

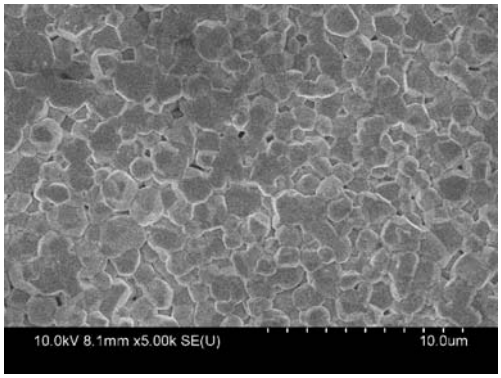

Fig. 5 The 8Y-SZ ceramic consolidated by the SPS with 5-min holds at 1250°C

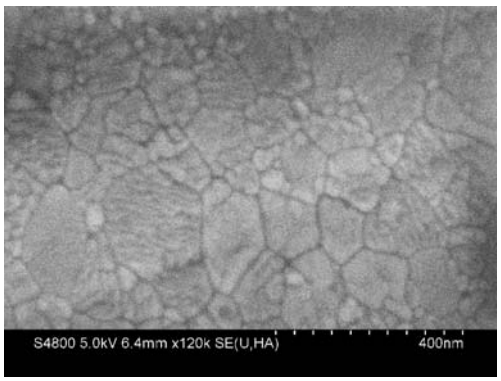

Fig. 6 The 8Y-SZ with 1 mass.% of the Al_2O_3 ceramic consolidated by the SPS with 5-min holds at 1150°C

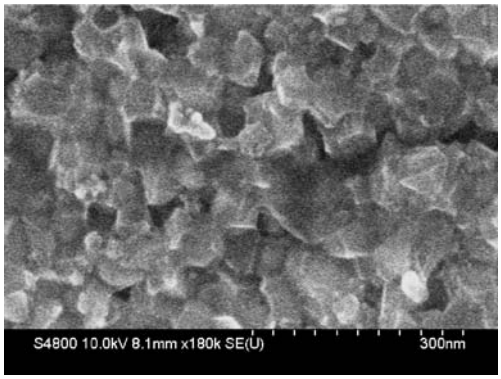

Fig. 7 The CGO ceramic consolidated by the SPS with 5-min holds at 1100°C

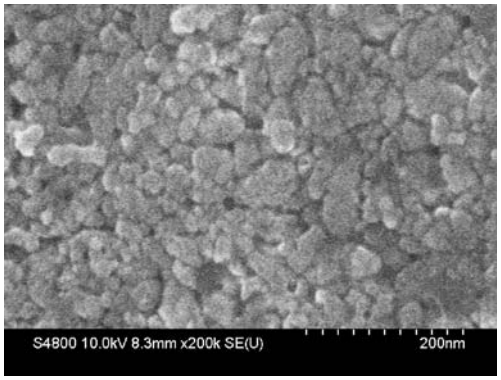

Fig. 9 The CGO ceramic consolidated by the SPS with 5-min holds at 1035°C

~89.2% and ~98.9% with an average grain size of 83 and 90 nm, respectively.

The relative densities of the CGO ceramic samples conslolidated with no preliminary CIPing from the $Gd_{20}Ce_{80}O_{1.90}$ powder (see Table 2) produced with no application of multiple nanoblasts and produced by nanoblast calcination and sintered at 1100 (heated to the holding temperatures at 500°C/min) were ~84.8% and ~89.1% with an average grain size of 161 and 79 nm, respectively. The relative densities of the CGO ceramic samples cold isostatically pressed from the $Gd_{20}Ce_{80}O_{1.90}$ powder produced with no application of multiple nanoblasts and sintered at 1100 and 1035°C (heated at 500°C/min) were ~92.3% and ~96.7% with an average grain size of 176 and 123 nm, respectively.

The SEM micrograph of the nanoblast CGO ceramic CIPed and consolidated by SPS at 1100°C for 5 min is shown on Fig. 7. This nano-grained ceramic was obtained because of using the $Gd_{20}Ce_{80}O_{1.90}$ sample CIPed from the nanosize powder (Fig. 4) produced by a nanoblast technique from engineered nanoreactors impregnated with $C_3H_6N_6O_6$. The relative density of this sample was ~93.8% and average grain size was ~73 nm. Similar to the consolidation of the 8Y-SZ ceramic, pretreatment by CIP at 400 MPa allowed a significant reduction of the SPS consolidation temperatures and increased relative density of the sintered ceramic.

The sintering behavior during SPS consolidation of preliminary CIPed CGO nanopowder synthesized from engineered nanoreactors with isothermal holding at 1035°C for 5 min and applied pressure evolution from 30 to 150 MPa is shown on Fig. 8. In this figure the relative densities are plotted as a function of the applied pressure, temperature and duration of isothermal holdings (numbers under each density value). As shown in Table 2, at this temperature the average grain size remained in the nano-scale range. The relative density of ceramic consolidated by SPS reached only ~83% during heating to 1000°C at an ambient pressure of ~65 MPa, and ~87.8% after heating to 1035°C while the pressure increased to approximately 90 MPa. Subsequent gradual increasing of applied pressure to 150 MPa during the final 5-min isothermal holds allowed reaching ~97% of relative density during only 3 min and ~98% after 5 min treatment (150 MPa). The SEM and TEM micrographs of the CGO ceramics

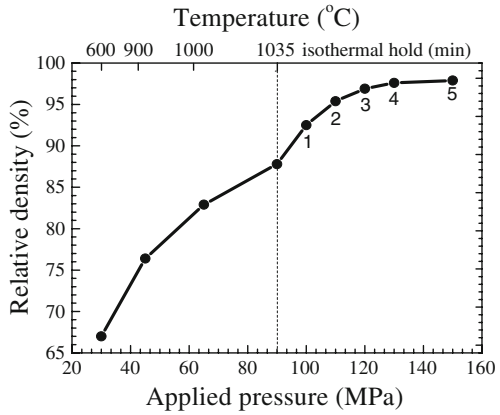

Fig. 8 SPS consolidation of preliminary CIPed CGO nanopowder synthesized from engineered nanoreactors (isothermal holds at 1035°C for 1 to 5 min)

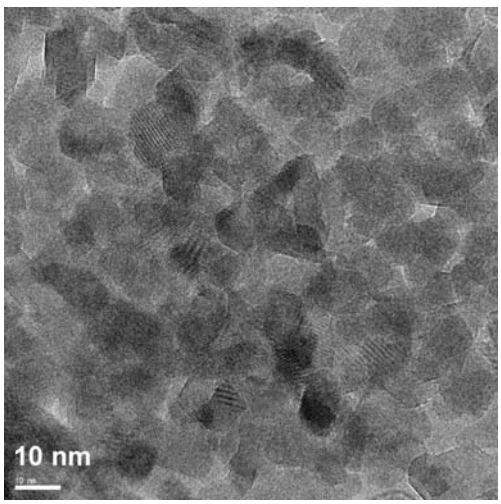

Fig. 10 The CGO ceramic consolidated by the SPS with 5-min holds at 970°C

consolidated by SPS at 1035°C and 970°C for 5 min are shown in Fig. 9 and 10, respectively. The extremely fine-grained highly dense nanoceramics were obtained by the SPS with 5-min holds at both temperatures (Table 2). As shown in Table 2, the relative densities of the CGO ceramic samples cold isostaticaly pressed and sintered at 1035 and 970°C (both heated to the hold temperature at 500°C/min) were ~97.9% and ~95.6% with a remarkable fine average grain size of 30 and 12 nm, respectively.

For all the above conditions, the sintering temperatures are several hundred degrees lower than the temperatures used in conventional sintering methods. Very limited grain growth was evident. Such fine grain size and narrow distribution well correspond with the average aggregate size of the initial powder. Also, the lower relative density at the higher hold temperatures well corresponds to the concurrence between the intraaggregate and interaggregate densifications at the different SPS regimes. It is possible to conclude, that due to rapid intraaggregate densification a residual intergrain porosity appears. In the case of lowering the hold temperatures, rearrangement of the primary crystallites into aggregates and crossaggregate rearrangement become slower and balanced, and total densification mainly determines by the applied external pressure.

It can be assumed that the morphological homogeneity of the starting powders for both 8Y-SZ and CGO plays a governing role in the success of the low-temperature SPS consolidation. Excluding the influence of agglomeration (due to morphological homogeneity of nano-aggregates) on the densification, plastic deformation should become of significant importance. This would support a densification mechanism based on grain boundary sliding and grain boundary rotation. That is why the pressure became of great importance during the isothermal stage of SPS through rearrangement of the crystallites and densification through plastic deformation.

4 Conclusions

The concept of the *in situ* engineering of nanoreactors—morphologically homogeneous aggregates of synthesized intermediate metastable products has been realized. The thermo-activated processes of nucleation-growth of the final compositions were realized within the preliminary localized volume of each single nanoreactor, which provides the heredity of the final structure of the nanosize products. This new approach of multimetal oxide nanosize powders engineering allowed the production of 8Y-SZ and CGO powders consisting of ~45 nm nano-aggregates with a remarkably homogeneous morphology.

The 8Y-SZ ceramic with average grain size of 90 nm and the CGO nanoceramic with an extremely fine grain microstructure were consolidated by low-temperature SPS under ambient pressures of 100–150 MPa. The CGO nano—ceramics with an average grain size of 73, 30 and 12 nm were obtained by SPS at 1100, 1035 and 970°C, respectively. Under these conditions, the sintering temperatures are much lower than the temperatures used in conventional sintering methods. Very limited grain growth was also evident. In addition, the significant role of sophisticatedly applied, unusually high pressure on the particle rearrangement through plastic or superplastic deformation was successfully demonstrated.

Such an accomplishment of our investigation opens the door to future investigations of the properties of bulk nanoceramics with such fine grain sizes that mesoscopic effects are anticipated.

References

1. Gleiter, Acta. Materialia **48**, 1–29 (2000)
2. Tjong, H. Chen, Mater. Sci. Eng. R. **45**, 1–88 (2004)
3. Johnston, P. Shah, Science **303**, 482–483 (2004)
4. Pileni, Nature Materials **2**, 145–150 (2000)
5. Millman, K. Bhatt, B. Prevo, O. Velev, Nature Materials **4**, 98–102 (2005)
6. Lee, S.-C. Choi, Mater. Lett. **58**, 390–393 (2004)
7. Vasylkiv, Y. Sakka, J. Ceram. Soc. Japan **109**, 500–505 (2001)
8. Vasylkiv, Y. Sakka, H. Borodians'ka, J. Am. Ceram. Soc. **86**, 299–304 (2001)
9. Vasylkiv, Y. Sakka, V. Skorokhod, J. Amer. Ceram. Soc. **89**, 1822–1826 (2003)
10. Tianshu, P. Hing, H. Huang, J. Kilner, Solid State Ionics **148**, 567–573 (2002)
11. Li, T. Ikegami, Y. Wang, T. Mori, Solid State Chem. **168**, 52–59 (2002)
12. Zhang, J. Ma, L. Kong, P. Hing, J. Kilner, Solid State Ionics **167**, 191–196 (2004)
13. Vasylkiv, T. Kolodiazhni, Y. Sakka, V. Skorokhod, J. Ceram. Soc. Japan **113**, 101–106 (2005)
14. Vasylkiv, Y. Sakka, J. Am. Ceram. Soc. **84**, 2489–2494 (2001)
15. Vasylkiv, Y. Sakka, Y. Maeda, V. Skorokhod, J. European Ceram. Soc. **24**, 469–473 (2004)
16. Ulrich, Chem. Eng. News **62**, 22–29 (1998)
17. Pratsinis, Prog. Energy Combust. Sci. **24**, 197–219 (1998)
18. Vasylkiv, Y. Sakka, Nano Letters **5**, 2598–2604 (2005)
19. Vasylkiv, Y. Sakka, V. Skorokhod, J. Amer. Ceram. Soc. **89**, 1822–1826 (2006)
20. Kuklja, J. Phys. Chem. B **105**, 10159–10162 (2001)
21. Shchukin, G. Sukhorukov, Adv. Mater. **16**, 671–682 (2004)
22. Angerer, L.G. Yu, K.A. Khor, G. Krumpel, Mat. Sci. Eng. A **381**, 16–19 (2004)
23. Olevsky, L. Froyen, Scripta Mater. **55**, 1175–1178 (2006)
24. Kakegawa, N. Uekawa, Y.J. Wu, Y. Sasaki, Mat. Sci. Eng. B **99**, 11–14 (2003)
25. Khor, X.J. Chen, S.H. Chan, L.G. Yu, Mat. Sci. Eng. A **366**, 120–126 (2004)
26. Chen, K.A. Khor, S.H. Chan, L.G. Yu, Mat. Sci. Eng. A **374**, 64–71 (2004)
27. Anselmi-Tamburini, J. Garay, Z. Munir, Scripta Mater. **54**, 823–828 (2006)